Journal of Thermal Analysis and Calorimetry, Vol. 94 (2008) 1, 169–174

THERMAL INVESTIGATION OF STRONTIUM ACETATE HEMIHYDRATE IN NITROGEN GAS

Y. Duan[1], *J. Li*[1], *X. Yang*[1], *X.-M. Cao*[1], *L. Hu*[1], *Z.-Y. Wang*[1], *Y.-W. Liu*[1,2*] *and C.-X. Wang*[1]

[1]College of Chemistry and Molecular Science, Wuhan University, Wuhan 430072, China
[2]College of Life Sciences, Wuhan University, Wuhan 430072, China

The thermal decomposition of strontium acetate hemihydrate has been studied by TG-DTA/DSC and TG coupled with Fourier transform infrared spectroscopy (FTIR) under non-isothermal conditions in nitrogen gas from ambient temperature to 600°C. The TG-DTA/DSC experiments indicate the decomposition goes mainly through two steps: the dehydration and the subsequent decomposition of anhydrous strontium acetate into strontium carbonate. TG-FTIR analysis of the evolved products from the non-oxidative thermal degradation indicates mainly the release of water, acetone and carbon dioxide. The model-free isoconversional methods are employed to calculate the E_a of both steps at different conversion α from 0.1 to 0.9 with increment of 0.05. The relative constant apparent E_a values during dehydration ($0.5<\alpha< 0.9$) of strontium acetate hemihydrate and decomposition of anhydrous strontium acetate ($0.5<\alpha<0.9$) suggest that the simplex reactions involved in the corresponding thermal events. The most probable kinetic models during dehydration and decomposition have been estimated by means of the master plots method.

Keywords: *master plots method, model-free isoconversional method, strontium acetate hemihydrate, TG-FTIR, thermal decomposition*

Introduction

The thermal decomposition of metal acetates are of great importance for their frequent application in the preparation of nano or complex material precursor. Their products which are obtained through precisely controlled calcination temperature and time in specific atmosphere, can be used as prospective materials for superior technical ceramics, materials for magnetic recording, many electronic components, sensor, catalysts as well as the high-temperature superconductors [1]. *d*-electron metal salts contain organic anions such as oxalates, acetates, formates etc. are common precursor systems for the controlled synthesis of *d*-metal oxides or alloys under mild condition [2].

A lot of studies have been performed for the thermal decomposition behavior of metal acetates by a variety of measurements such as TG/DTG, DTA, DSC and TG coupled with FTIR or MS (mass spectroscopy), etc. [3–10]. Recently thermal analysis coupled with EGA has been developed rapidly and are frequently used for the quantification of each single gaseous evolution process as the result of an increasing thermal ramp or a defined isothermal temperature. Compared with conventional methods, the coupled technique offers an invaluable interpretation to reveal the possible degradation mechanism in the thermal events. The thermal analysis coupled with EGA reviews can be seen in literatures [11, 12].

The model-fitting method and the model-free method are the two primary computational methods to determine the 'kinetic triplets' of the decomposition processes. Vyazovkin and Wight pointed out that the use of the model-free approach is recommended as a trustworthy way of obtaining reliable and consistent kinetic information from both non-isothermal and isothermal data [13–16].

In present work, an investigation of thermal decomposition of strontium acetate hemihydrate was carried out under non-isothermal condition from ambient to 600°C in N_2 atmosphere via TG-DTA/DSC, DSC, TG-FTIR and XRD techniques. Simultaneous techniques of coupling TG and FTIR were utilized to monitor the gas released from the decomposition process. The kinetics of the non-isothermal dehydration and decomposition of strontium acetate was also studied. The kinetic parameters were obtained by the model-free isoconversional method and the master plots method [17].

Theoretical

For a reaction under non-isothermal condition, its kinetic function can be expressed as the following form [18]:

$$g(\alpha)=\frac{AE_a}{\beta R}P(u) \qquad (1)$$

where α is an extent of conversion, β the heating rate, E_a the apparent activation energy, R the gas constant, A pre-exponential factor, $g(\alpha)$ the integral expression of kinetic model function, and

* Author for correspondence: ipc@whu.edu.cn

1388–6150/$20.00

Akadémiai Kiadó, Budapest, Hungary
Springer, Dordrecht, The Netherlands

$$P(u)=\int_{\infty}^{u}-\left(\frac{e^{u}}{u^{2}}\right)\mathrm{d}u$$

where $u=E_a/RT$.

Because the exponential integral, $P(u)$, has no analytical solution. An approximation formula of high accuracy [19] was used.

$$-\ln P(u)=0.37773896+1.89466100\ln u+1.00145033u \quad (2)$$

Inserting Eq. (2) in Eq. (1) , one can obtain:

$$\ln\left[\frac{\beta}{T^{1.89466100}}\right]=\left\{\ln\left[\frac{AE_a}{Rg(\alpha)}\right]+3.63504095-1.89466100\ln E_a\right\}-1.00145033\frac{E_a}{RT} \quad (3)$$

The first term at the right side of Eq. (3) is a constant corresponding to a given value of α. So for a series of experiments at different heating rates, the plot of $\ln(\beta/T^{1.89466100})$ *vs.* $1/T$ with the same conversional ratio should be a line with the slope of $-1.00145033E_a/R$. Then, the apparent activation energy E_a can be calculated from the slope.

Inserting α=0.5 into Eq. (1), one can get

$$g(0.5)=\frac{AE_a}{\beta R}P(u_{0.5}) \quad (4)$$

where $u_{0.5}=E_a/RT_{0.5}$, $T_{0.5}$ is the temperature when α equals to 0.5. When Eq. (1) is divided by Eq. (4), the following equation is obtained:

$$g(\alpha)/g(0.5)=P(u)/P(u_{0.5}) \quad (5)$$

By plotting $g(\alpha)/g(0.5)$ *vs.* α corresponds to different theoretical model functions, the theoretical master plots can be obtained for different kinetic mechanism. With E_a calculated from Eq. (3), the experimental master plots of $P(u)/P(u_{0.5})$ *vs.* α could be drawn from the experimental data obtained under different heating rates. Equation (5) indicates that, for arbitrary α, the experimental value $P(u)/P(u_{0.5})$ and theoretically calculated values of $g(\alpha)/g(0.5)$ are equivalent when an appropriate kinetic model is used. So this integral master plots method can be used to determine the most probable mechanism function.

Then, the pre-exponential factor A can be obtained from the slope of the plot of $g(\alpha)$ *vs.* $E_aP(u)/\beta R$.

Experimental

Strontium acetate hemihydrate powder (analytical grade) was purchased from Beijing Reagent Factory without further purification.

TG experiments were carried out on a Setaram Setsys 16 TG-DTA/DSC thermal analyzer (France). Instrument calibration was performed with standard indium, tin, lead, zinc, silver and gold sample of known melting temperature. All standards were of purity≥99.99%. For the kinetics measurement about 5 mg sample was weighted into an open alumina crucible. The furnace temperature was programmed to rise from ambient temperature to 600°C at the rates of 5, 10, 15 and 20 K min^{-1}. Nitrogen gas of high purity (purity≥99.999%) was used as carrier gas at flow rate of 50 mL min^{-1}.

Simultaneous TG coupled with FTIR was done on the Setaram Setsys 16 TG-DTA/DSC Instrument and a Thermo Nicolet Nexus 670 Fourier Transform Infrared Spectrometer. About 10 mg sample was loaded into an open alumina crucible. The heating rate of TG furnace was 20 K min^{-1} and nitrogen gas of high purity (purity≥99.999%) with a flow rate of 100 mL min^{-1} was used as carrier gas. The sample was heated from ambient temperature to 600°C. The transfer line used to connect TG and FTIR was a 1 m long stainless steel tube with an internal diameter of 2 mm, of which the temperature is maintained at 200°C. The TG accessory of the IR Spectrometer was used, which has a 45 mL gas cell with a 200 mm path length. It was also heated at the constant temperature of 200°C. The IR spectra were collected at 8 cm^{-1} resolution, co-adding 8 scans per spectrum. This resulted in a temporal resolution of 4.32 s. Lag time that the gas products went from furnace to gas cell was about 7 s. The FTIR spectra have been identified based on the FTIR reference spectra available on the World Wide Web in the libraries of NIST [20].

The differential scanning calorimetry (DSC) measurements were performed on a Mettler-Toledo calorimeter, model DSC 822^e. About 6 mg sample was added in the aluminium sample pan. The reference pan was empty. The DSC experiments were run at the heating rate and cooling rate of 10 K min^{-1}.

X-ray diffraction (XRD) patterns were recorded on Bruker D8 (Germany) model X-ray diffractometer with a graphite monochromator and CuK_α and scan rate of 4° min^{-1}.

Results and discussion

TG/DTG-DSC and DSC analysis

The results of TG experiments carried out in N_2 under 600°C at the heating rates of 5, 10, 15 and 20 K min^{-1} are shown in Fig. 1. It can be observed that the mass losses of each step are almost identical at different heating rates. The TG curves and DTG peaks were gradually shifting to the right accompanied with increase of heating rates. The TG/DTG-DSC curves obtained at heating rate of 10 K min^{-1} is presented in Fig. 2, which displayed $Sr(AC)_2\cdot 0.5H_2O$ thermally

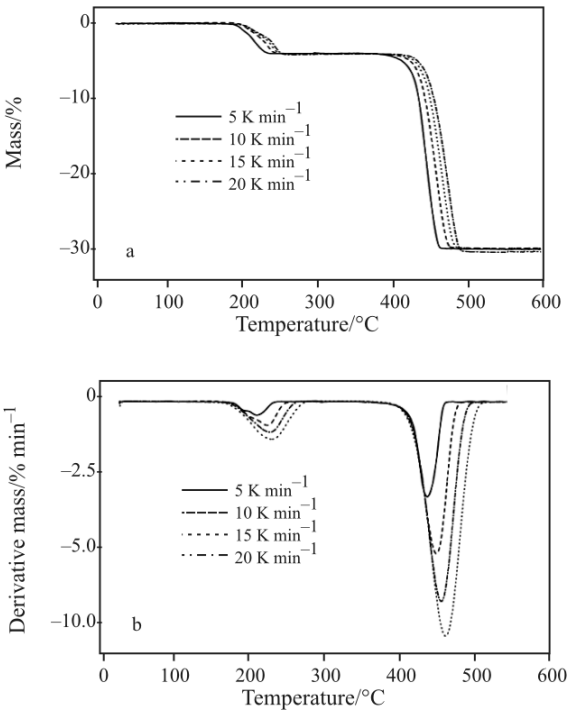

Fig. 1 a – TG and b – DTG curves for the decomposition of $Sr(AC)_2 \cdot 0.5H_2O$ at different heating rate, N_2 flow rate 50 mL min^{-1}

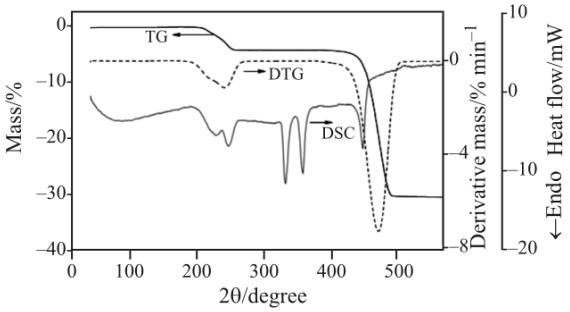

Fig. 2 TG-DTG-DSC curves for the decomposition of $Sr(AC)_2 \cdot 0.5H_2O$ at 10 K min^{-1}, N_2 flow rate 50 mL min^{-1}

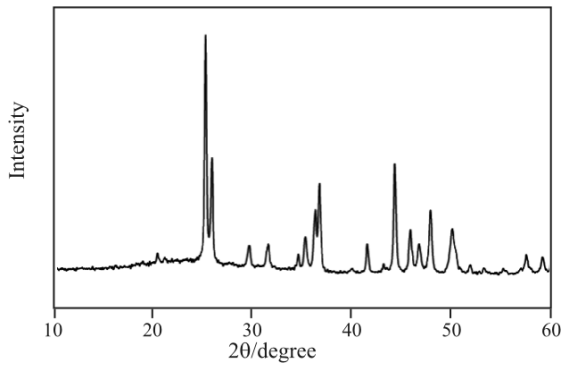

Fig. 3 X-ray powder diffraction patterns of final decomposition product of $Sr(AC)_2 \cdot 0.5H_2O$ in N_2 at ambient temperature

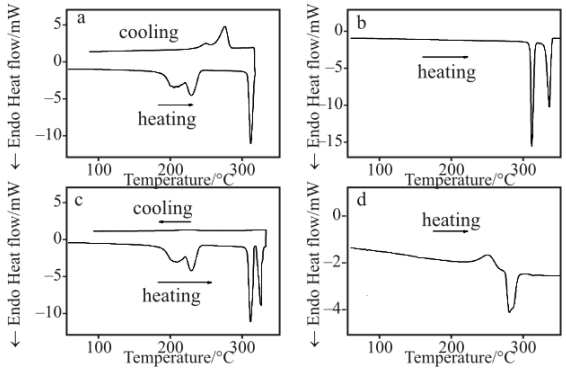

Fig. 4 DSC curves of $Sr(AC)_2 \cdot 0.5H_2O$ a – heated from 30 to 323°C and cooled to 30°C, b – rescan a heated from 30 to 360°C, c – heated from 30 to 360°C and cooled to 30°C, d – rescan c from 30 from 360°C

decomposed mainly through two-step mass losses. The first step of mass loss 4.11% agreed with the theoretical value 4.16% between 180 to 260°C was attributed to the dehydration of $Sr(AC)_2 \cdot 0.5H_2O$. Two overlapped endothermic peaks with maximum values 213.1 and 231.9°C of the dehydration process can be seen in the DSC curves. This implies that the dehydration occurs in at least two stages, which is verified by the DTG curves at different heating rates presented in Fig. 1b. The second step of mass loss 26.92% agreed with theoretical value 27.10% between 400 to 480°C can be assigned to the decomposition of anhydrous $Sr(AC)_2$ to $SrCO_3$. A sharp endothermic peak at 430.6°C and a broad exothermic peak between 440 and 500°C in the DSC curve superimposed upon the decomposition process. The XRD experiment was carried out for the final decomposition product of $Sr(AC)_2 \cdot 0.5H_2O$ at ambient temperature. The result (shown in Fig. 3) conformed very closely to the standard XRD patterns of $SrCO_3$ (JCPDS No. 87-1778).

Figure 2 shows that there were two sharp endothermic peaks with maximum values of 314.3 and 331.6°C in DSC curve with no corresponding mass loss in TG curve suggests two-phase change processes occurred in this temperature range. In order to identify nature of the two sharp DSC peaks, DSC experiments (shown in Fig. 4) were carried out at the heating rate and cooling rate of 10 K min^{-1}. In Fig. 4a, the DSC experiment was firstly heated from 30 to 323°C which just exceeded the first phase change and the second phase change was not taken place, then cooled down to ambient temperature. Figure 4b shows the rescan of the sample in Fig. 4a. The sharp DSC peak at about 314°C appeared again in the rescan DSC curve indicated that the broad peak appeared during the cooling process between 250–290°C in Fig. 4a can be assigned to the solidification or recrystallization and the former phase change peak was the endothermal melting process. In

Fig. 4c, the similar DSC run was done as Fig. 4a except for the higher terminated temperature 360°C which just exceeded the second phase change, there was no endotherm or exotherm peak during the cooling process. Figure 4d shows the rescan of the sample in Fig. 4c, there presented a broad exothermal peak between 230 to 270°C and followed an endothermal peak between 270 to 300°C which may due to the crystallization peak and the melting of the new crystalline of anhydrous $Sr(AC)_2$, respectively. McAdie [21] have reported that the endothermal fusion of the anhydrous strontium acetate occurs at 321±1°C (peak temperature), with no other enthalpic or mass changes being observed between dehydration and fusion. The dissimilar observations may lie in the different resolution of the apparatus being used.

TG-FTIR analysis

By utilization of TG coupled with evolved gas analysis (EGA), the nature of volatile products released by a substance subjected to a controlled temperature program are on-line determined, with the possibility to proven a supposed reaction, either under isothermal or under heating conditions [7]. The evolved gaseous species are analyzed by FTIR. The 3D plot FTIR gas spectra from the thermal decomposition process of $Sr(AC)_2{\cdot}0.5H_2O$ is presented in the Fig. 5. The characteristic bands at 1700–1500 and 3740–3500 cm^{-1} can be assigned to the bending vibration and stretching vibration of O–H which corresponding to the dehydration of $Sr(AC)_2{\cdot}1/2H_2O$ in the range of 180–260°C. Carbon dioxide was easily identified by the characteristic peak at 2358 cm^{-1} during 400–480°C. The FTIR spectra observed at the Gram Schmidt peak temperature (442.1°C) is shown in Fig. 6. By comparing with NIST database, the gases evolved at 442.1°C were identified as a mixture of gaseous acetone and minor carbon dioxide. The same result was also obtained by Borger *et al.* [22].

In Fig. 7, it shows that the plot of TG/DTG/total IR intensity of decomposition of strontium acetate

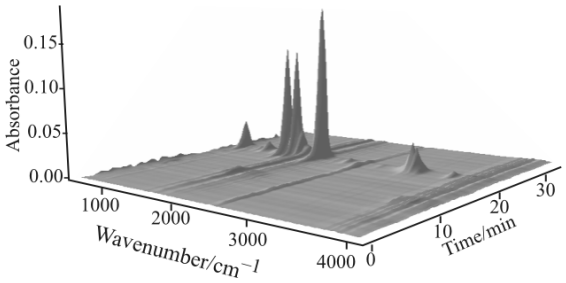

Fig. 5 The 3D surface graph for the FTIR spectra of the evolved gases produced by $Sr(AC)_2{\cdot}0.5H_2O$ decomposition at heating rate 20 K min^{-1} and N_2 flow rate 100 mL min^{-1}

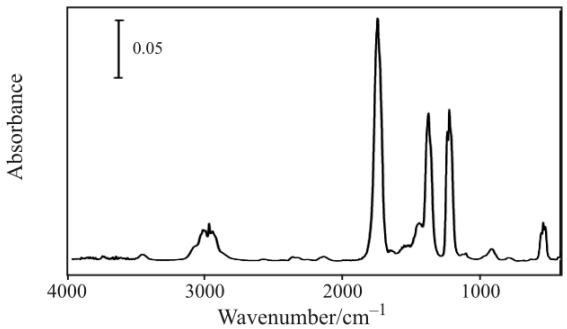

Fig. 6 The compared FTIR spectra of evolved gases from $Sr(AC)_2{\cdot}0.5H_2O$ in N_2 measured at 442.1°C

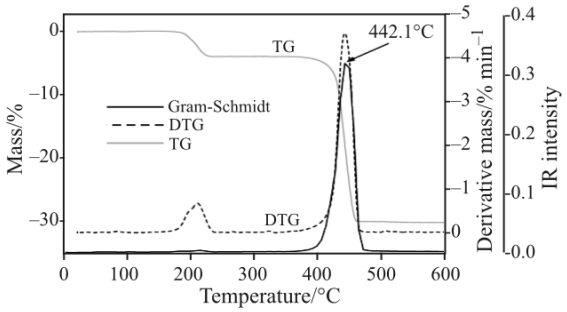

Fig. 7 The curves of TG, DTG and the total FTIR absorbance intensity of evolved gases, gotten during the $Sr(AC)_2{\cdot}0.5H_2O$ decomposition process by TG-FTIR, heating rate 20 K min^{-1}, N_2 flow rate 100 mL min^{-1}

hemihydrate at the heating rate 20 K min^{-1} and N_2 flow rate 100 mL min^{-1}. With consideration of lag time from furnace to gas cell, the DTG peaks of mass loss is well corresponding to peaks of the IR intensity during both the dehydration and decomposition of strontium acetate.

The plots of IR absorbance at several characteristic wavenumbers *vs.* temperature are shown in Fig. 8 which indicated the changing of the evolution rates with temperature for each gaseous product. The peak temperatures which represent the temperatures of the maximum evolution rates show that the water is the gaseous product of the first stage mass loss, while minor carbon dioxide and acetone are the gaseous products of the second stage mass loss.

In addition, the corresponding decomposition processes can be summarized in the following steps:

$$Sr(CH_3COO)_2{\cdot}0.5H_2O(s)\rightarrow Sr(CH_3COO)_2(s)+0.5H_2O(g)$$

$$Sr(CH_3COO)_2(s)\xrightarrow{\text{fusion}}Sr(CH_3COO)_2(l)\xrightarrow{\text{structural change}}$$
$$Sr(CH_3COO)_2(l)\rightarrow SrCO_3(s)+CH_3COCH_3(g)+CO_2(g)$$

Model-free isoconversional method to obtain the activation energy E_a

With Eq. (3), by plotting $\ln(\beta/T^{1.89466100})$ *vs.* $1/T$ at different heating rates and α, values of the apparent acti-

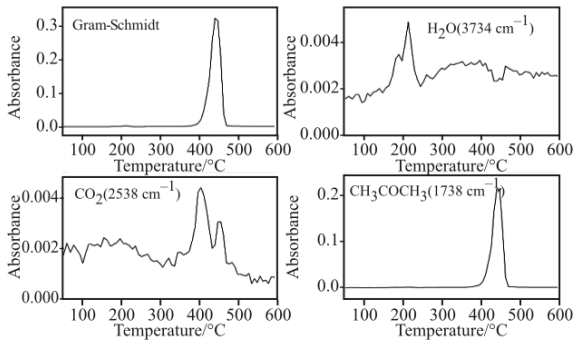

Fig. 8 IR absorbance *vs.* temperature curves of identified evolved gaseous species evolved from $Sr(AC)_2 \cdot 0.5H_2O$ decomposed in N_2, measured by online-coupled TG-FTIR system (heating rate 20 K min^{-1}, N_2 flow rate 100 mL min^{-1})

vation energy E_a are obtained and shown in Fig. 9. In the dehydration process, the E_a decreased from 198.0 to 129.5 kJ mol^{-1} when conversion $0.1<\alpha<0.5$ and remained constant with values of 133.4±6.6 kJ mol^{-1} in the range $0.5<\alpha<0.9$. The evidence of an inflection point on the mass loss curves supports the concept of a two-stage type of water loss. At the same time, the doublet DSC endothermal peaks during dehydration may represent separation of two modes of bonding of water molecules with the strontium acetate lattice. Unfortunately, lattice structures of $Sr(AC)_2 \cdot 0.5H_2O$ required for further interpretation have not been found. Similar to the dehydration process, the E_a during decomposition when conversion $0.1<\alpha< 0.5$ presented a decreased from 254.7 to 215.5 kJ mol^{-1} and kept constant with values of 210.6±2.9 kJ mol^{-1} in the range $0.5<\alpha< 0.9$. Though the single DTG peak exists during the decomposition, the two superimposed DSC peaks and the variation of E_a suggest the occurrence of multiplex reaction. McAdie [21] considered that the liberation of acetone occurs with endothermal process initially, however thermal degradation of the liberated organic fragment gives rise to considerable exothermal activity superimposed upon the decomposition process.

The obtained relative constant values of E_a during dehydration of $Sr(AC)_2 \cdot 0.5H_2O$ and decomposition of liquid anhydrous $Sr(AC)_2$ indicate a high probability of a single-step mechanism.

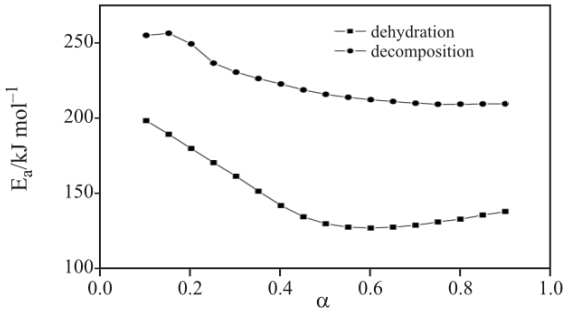

Fig. 9 The E_a of dehydration and decomposition process determined by model-free isoconversional method

Determination of the kinetic models of dehydration and decomposition process

The data analysis was carried out by means of master plot methods [23]. The conventional model functions [24] are well known equations.

It is worth noting that the two-phase changes have taken place prior to the decomposition of anhydrous $Sr(AC)_2$. So the decomposition occurred in the form of liquid state $Sr(AC)_2$ whose process can be assigned to the homogeneous reaction. It is more reasonable to descript this reaction by the simple order reaction model.

According to Eqs (4) and (5), plotting $g(\alpha)/g(0.5)$ *vs.* α corresponds to theoretical master plots of various $g(\alpha)$ functions. To draw the experimental master plots of $P(u)/P(u_{0.5})$ *vs.* α from experimental data obtained under four heating rates, the knowledge of temperature as a function of α and the value of E_a for the process should be known in advance, and $P(u)$ can be calculated directly using numerical Simpson's procedure or some approximate formulas (Eq. (2)). Both of the experimental and the theoretical master plots are shown in Fig. 10. For a

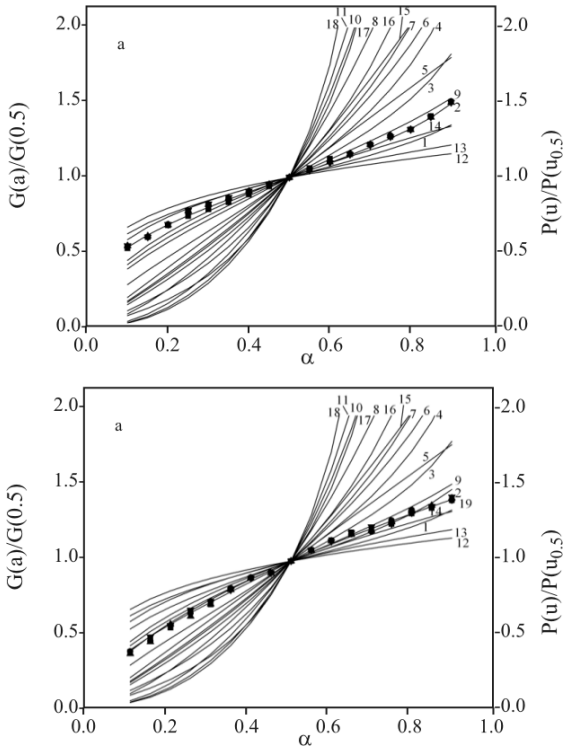

Fig. 10 The theoretical master plots (—) and the experimental master plots at heating rates of ▼ – 5, ▲ – 10, ● – 15 and ■ – 20 K min^{-1} for a – dehydration($0.5<\alpha<0.9$) and b – decomposition ($0.5<\alpha<0.9$) in flowing N_2

Table 1 Kinetic triplets during the dehydration ($0.5<\alpha< 0.9$) and decomposition process ($0.5<\alpha< 0.9$)

Reaction	E/kJ mol^{-1}	ln$A$/s^{-1}	n	model function/$g(\alpha)$
dehydration	133.4±6.6	27.50±0.11	3	$[-\ln(1-\alpha)]^{1/3}$
decomposition	210.6±2.9	13.18±0.04	0.62	$\frac{1-(1-\alpha)^{1-0.62}}{1-0.62}$

given α, the experimental value of $P(u)/P(u_{0.5})$ and theoretically calculated values of $g(\alpha)/g(0.5)$ are equivalent when an appropriated kinetic model is used. The experimental plots related to different heating rates are nearly identical.

Finally, we obtain the kinetic models of Avrami–Erofeev (A_3) mechanism during dehydration of $Sr(AC)_2{\cdot}0.5H_2O$ ($0.5<\alpha<0.9$) and 0.62 order reaction during decomposition ($0.5<\alpha<0.9$) of liquid anhydrous $Sr(AC)_2$. The Avrami–Erofeev mechanism implies that the process in the conversion range of $0.5<\alpha<0.9$ is regulated by nucleation and growth processes at the surfaces of the crushed crystals [25]. The non-integral order of 0.62 order reaction indicates a mixture reactions maybe involved in the system [26]. After the mechanism function $g(\alpha)$ is confirmed, according to Eq. (1) , plotting $g(\alpha)$ *vs.* $E_aP(u)/\beta R$ at different heating rate, the pre-exponential factor ln$A$ is obtained. The corresponding kinetic triplets are tabulated in Table 1.

Conclusions

The thermal decomposition of $Sr(AC)_2{\cdot}0.5H_2O$ in N_2 under 600°C was investigated by TG-DTA/DSC-FTIR. Two main mass loss steps are observed: dehydration and decomposition of anhydrous $Sr(AC)_2$ to $SrCO_3$. Two-phase changes have been observed between dehydration and decomposition. The TG-FTIR experiment shows us important information about the online gaseous products during the thermal event. On the basis of gases involved, the decomposition process of $Sr(AC)_2{\cdot}0.5H_2O$ has been postulated. Kinetics studies by model-free isoconversional method indicate that the dehydration ($0.5<\alpha<0.9$) of $Sr(AC)_2{\cdot}0.5H_2O$ and decomposition ($0.5<\alpha<0.9$) of liquid anhydrous $Sr(AC)_2$ obey the corresponding simple mechanism. The kinetic models have been estimated with the master-plot method.

Acknowledgements

This work was financially supported by the National Nature Sciences Foundation of China (Grant No. 20373050, No. 30600116), Nature Sciences Foundation of Hubei and China Postdoctoral Science Foundation.

References

1 M. A. Gabal, Thermochim. Acta, 402 (2003) 199.
2 B. Malecka, J. Therm. Anal. Cal., 78 (2004) 535.
3 M. D. Judd, B. A. Plunkett and M. I. Pope, J. Thermal Anal., 6 (1974) 555.
4 N. Koga and H. Tanaka, Solid State Ionics, 44 (1990) 1.
5 M. Afzal, P. K. Butt and H. Ahmad, J. Thermal Anal., 37 (1991) 1015.
6 M. C. Ball and L. Portwood, J. Thermal Anal., 41 (1994) 347.
7 T. Arii and Y. Masuda, Thermochim. Acta, 342 (1999) 139.
8 K. Zhang, J. Hong, G. Cao, D. Zhan, Y. Tao and C. Cong, Thermochim. Acta, 437 (2005) 145.
9 A. G. B. de Cruz, J. L. Wardell and A. M. Rocco, Thermochim. Acta, 443 (2006) 217.
10 V. Logvinenko, O. Polunina, Yu. Mikhailov, K. Mikhailov and B. Bokhonov, J. Therm. Anal. Cal. 90 (2007) 813.
11 S. Materzaai, A. Gentili and R. Curini, Talanta, 68 (2006) 489.
12 S. Materzaai, A. Gentili and R. Curini, Talanta, 69 (2006) 781.
13 S. Vyazovkin and C. A. Wight, Annu. Rev. Phys. Chem., 48 (1997) 125.
14 S. Vyazovkin, Int. Rev. Phys. Chem., 19 (2000) 45.
15 S. Vyazovkin and C. A. Wight, Thermochim. Acta, 340-341 (1999) 53.
16 S. Vyazovkin, Thermochim. Acta, 355 (2000) 155.
18 X.-M. Cao, J. Therm. Anal. Cal., OnlineFirst DOI:10.1007/s10973-007-8574-X.
18 J. Li, Z. Wang, X. Yang, L. Hu, Y. Liu and C. Wang, Thermochim. Acta, 447 (2006) 147.
19 W. Tang, Y. Liu, H. Zhang and C. Wang, Thermochim. Acta, 408 (2003) 39.
20 NIST Chemistry Webbook standard reference database No. 69, June 2005 Release.
21 H. G. McAdie, J. Inorg. Nucl. Chem., 28 (1966) 2801.
22 A. Borger, H. Dallmann and H. Langbein, Thermochim. Acta, 387 (2002) 141.
23 F. J. Gotor, J. M. Criado, J. Malek and N. Koga, J. Phys. Chem. A, 104 (2000) 10777.
24 V. Mamleev, S. Bourbigot, M. L. Bras, S. Duquesne and J. Šesták, Phys. Chem. Chem. Phys., 2 (2000) 4708.
25 N. Koga and H. Tanaka, Thermochim. Acta, 303 (1997) 69.
26 R. L. Remmele, J. J. Zhang-van Enk, V. Dharmavaram, D. Balaban, M. Durst, A. Shoshitaishvili and H. Rand, J. Am. Chem. Soc., 127 (2005) 8328.

Received: November 17, 2007
Accepted: April 23, 2008
OnlineFirst: August 15, 2008

DOI: 10.1007/s10973-007-8711-6